Fast Analytic Electromigration Analysis for General Multisegment Interconnect Wires

Liang Chen, *Student Member, IEEE*, Sheldon X.-D. Tan, *Senior Member, IEEE*, Zeyu Sun, *Student Member, IEEE*, Shaoyi Peng, *Student Member, IEEE*, Min Tang, *Member, IEEE*, and Junfa Mao, *Fellow, IEEE*

***Abstract*— Electromigration (EM) is considered to be one of the most important reliability issues for current and future ICs in 10-nm technology and below. In this article, we propose a fast analytic solution to compute the stress evolution in the confined multisegment interconnect wires. The new method, called the accelerated separation of variables (ASOV) method, aims to find the analytic solutions of the partial differential equations of stress in confined interconnect metals based on the SOV method. It offers several improvements over the existing plain SOV-based method. First, we show that the accuracy of the solution depends on the structure of the interconnects. As a result, the number of required eigenvalues is structure and problem dependent, instead of fixed numbers used by the existing SOV method. Second, for the straight line multisegment and star-structured multiterminal interconnects, analytical expressions are formulated to calculate the eigenvalues directly instead of using numerical methods as in the existing SOV method. Third, we propose a linear Gaussian elimination (GE) algorithm by exploiting the banded structure with the serrated-edge form of the transcendental matrix, which can significantly speed up GE process, and is the key computing step in the SOV-based solution framework. Fourth, instead of using the simple bisection search, we propose to use an enhanced determinant-based secant iterative method to find the eigenvalues of the transcendental matrix. Numerical results show that a good agreement is achieved between analytical and numerical results on two special cases, and the resulting algorithm can lead to 3–5X speedup over the existing plain SOV-based solution on a number of multisegment interconnects benchmarks.**

***Index Terms*— Analytical expressions, eigenvalues, electromigration (EM), Gaussian elimination (GE), secant method, separation of variables (SOV) method, Wittrick–Williams (WW) algorithm.**

Manuscript received June 16, 2019; revised August 10, 2019; accepted September 3, 2019. Date of publication September 27, 2019; date of current version January 21, 2020. This work was supported in part by the National Science Foundation (NSF) under Grant CCF-1527324, Grant CCF-1816361, and Grant OISE-1854276. The work of L. Chen was supported by the China Scholarship Council under Grant 201806230078. *(Corresponding author: Sheldon X.-D. Tan.)*

L. Chen is with the Key Laboratory of Ministry of Education of China for Research of Design and Electromagnetic Compatibility of High Speed Electronic Systems, Shanghai Jiao Tong University, Shanghai 200240, China, and also with the Department of Electrical and Computer Engineering, University of California at Riverside, Riverside, CA 92521 USA (e-mail: chenliang_sjtu@sjtu.edu.cn).

S. X.-D. Tan, Z. Sun, and S. Peng are with the Department of Electrical and Computer Engineering, University of California at Riverside, Riverside, CA 92521 USA (e-mail: stan@ee.ucr.edu).

M. Tang and J. Mao are with the Key Laboratory of Ministry of Education of China for Research of Design and Electromagnetic Compatibility of High Speed Electronic Systems, Shanghai Jiao Tong University, Shanghai 200240, China.

Color versions of one or more of the figures in this article are available online at http://ieeexplore.ieee.org.

Digital Object Identifier 10.1109/TVLSI.2019.2940197

I. Introduction

ELECTROMIGRATION (EM) has become one of the most critical design issues and limiting factors for nanometer VLSI designs because of the shrinking size and increasing current density of the interconnects as technology scales down to deep nanometers. As a result, EM verification became a critical step for chip signoff. It was well known that existing Black- and Blech-based EM models are subject to growing criticism due to their over conservativeness, which leads to excessive design guard band [1].

Recently, a number of physics-based EM models and assessment techniques have been proposed [1]–[14]. These EM models are primarily based on the hydrostatic stress diffusion kinetics in the confined metal wires and, therefore, have a more accurate time-to-failure estimation for general interconnect wires over a wide range of stress conditions. However, finding the solutions to Korhonen's differential equations for complex on-chip interconnect networks requires high computational cost by using numerical methods such as finite difference method (FDM) [10], [15], [16] and finite element analysis (FEA) [13]. This is because numerical methods cannot avoid discretization of space and time, which increase the number of unknown variables significantly.

In order to facilitate the EM reliability assessment for large interconnect trees, several analytical solutions have been developed to solve the diffusion-like partial differential equations (PDEs), describing the dynamic hydrostatic stress. Korhonen *et al.* [17] first proposed an analytical solution for a single wire, which is the simplest interconnect structure. Recently, based on the Laplace transformation technique, the analytical expressions were provided to describe the hydrostatic stress evolution in star-structured multiterminal interconnects such as the straight-line three-terminal wires, the T-shaped four-terminal wires, and the cross-shaped five-terminal wires. Then, an integral transform technique [18] was employed to solve 1-D Korhonen's equation for straight line multisegment interconnects with different current densities. However, the aforementioned methods are only suitable for specific interconnect structures, not for general multisegment interconnect trees. In order to estimate the transient hydrostatic stress evolution for general interconnect networks, a separation of variables (SOV) method [19] based on eigenvalues and eigenfunctions was proposed to address the 2-D interconnect

1063-8210 © 2019 IEEE. Personal use is permitted, but republication/redistribution requires IEEE permission.
See https://www.ieee.org/publications/rights/index.html for more information.

Authorized licensed use limited to: Univ of Calif Riverside. Downloaded on June 24,2026 at 00:43:07 UTC from IEEE Xplore. Restrictions apply.

tree structures. Afterward, another analytic solution for a single wire with inhomogeneous boundary conditions (BCs), which considers the temperature-induced migration effects, was obtained through an integrating factor technique [14]. In this article, we mainly focus on the SOV method [19], which can be applied for more general multisegment interconnects. The existing SOV-based method, however, computes eigenvalues numerically using the Wittrick–Williams (WW) algorithm [19], which costs the most time especially for large interconnects as shown in this article. As a result, more efficient approaches to determine the eigenvalues are highly desirable to further improve this existing SOV method.

In this article, we propose a new analytic solution to compute the stress evolution over time in the confined multisegment interconnect wires. The new method is still based on the SOV solution framework to solve the PDEs of stress. The proposed method has few important improvements over the exiting SOV method. Our new contributions are given as follows.

1) We show that the accuracy of the solution depends on the structure of the interconnects. As a result, the number of required eigenvalues is structure and problem-dependent, instead of fixed numbers used by the existing SOV method.
2) We derive the analytic formula for eigenvalues of the straight line multisegment and star-structured multiterminal interconnects in VLSI layout instead of using numerical methods as in existing SOV method. As a result, more efficient analytic solutions can be derived for those multisegment interconnects.
3) We propose a linear Gaussian elimination (GE) algorithm by exploiting the banded structure with the serrated-edge form of the transcendental matrix. The resulting solver can lead to better performance than the general sparse GE process.
4) Instead of using the simple bisection search to find the roots in the transcendental matrix, we propose to use determinant-based secant method for searching the roots or eigenvalues of the transcendental matrix. Such a secant-based root search algorithm leads to CPU time reduction for the proposed analytic solution to EM analysis.

Numerical results show that the resulting algorithm can lead to 3–5X speedup over the existing SOV-based solution on a number of multisegment interconnects benchmarks. The rest of this article is organized as follows. Section II reviews the recently proposed physics-based EM models and existing SOV-based solutions. We also highlight the major computing bottlenecks of the existing SOV method. Section III presents our new analytic solutions to the eigenvalues for straight line and star-structured multisegment interconnects. Section IV presents the new accelerated SOV (ASOV) solution for EM stress analysis for general multisegment interconnect wires. Section V presents the numerical results for the proposed method and comparison against existing works. Section VI concludes this article.

II. Review of EM and an Analytical Electromigration Model

A. Physics-Based EM Modeling

EM is a physical phenomenon of the migration of metal atoms along a direction of the applied electrical field [20], [21]. The momentum exchange between atoms and the conducting electrons results in metal density depletion at the cathode and a corresponding metal accumulation at the anode ends of the metal wire. Since the thin layers of refractive metals form diffusion barriers for Cu atoms preventing them from diffusing into interlayer dielectrics (ILD) and intermetal dielectrics (IMD), the EM occurs primarily on the interconnect tree, which is a continuously connected, highly conductive metal within one layer of metallization, terminated by diffusion barriers. When a metal wire is embedded into a rigid confinement, the wire volume changes induced by the atom depletion and accumulation due to migration create tension at the cathode end and compression at the anode end of the wire. The lasting electrical load increases these stresses, as well as the stress gradient along the metal wire. The stress generated inside the embedded metal wire is a prime cause of the void and hillock formation at the opposite ends of the wire [1], [22], [23]. Degradation of the electrical resistance of the interconnect segment can be derived from the solution of kinetics equation describing the time evolution of stress in the interconnect segments [17]. The void nucleation time could be obtained when stress reaches the critical value σ_{crit} and extracted kinetics of the void volume evolution governs the evolution of wire resistance [24].

The physics-based analytical model considering the void nucleation and kinetics of void size evolution was proposed by Korhonen *et al.* [17] and further developed by other researchers. For a general interconnect wires with n nodes, including p interior junction nodes $x_r \in \{x_{r1}, x_{r2}, \ldots, x_{rp}\}$ and q block terminals $x_b \in \{x_{b1}, x_{b2}, \ldots, x_{bq}\}$, the hydrostatic stress distribution $\sigma(x,t)$ along the wire is described by the following Korhonen's equation:

$$\begin{aligned}
&\frac{\partial \sigma_{ij}(x,t)}{\partial t} = \frac{\partial}{\partial x}\left[\kappa_{ij}\left(\frac{\partial \sigma_{ij}(x,t)}{\partial x} + G_{ij}\right)\right], \quad t > 0 \\
&\text{BC}: \sigma_{ij_1}(x_i,t) = \sigma_{ij_2}(x_i,t), t > 0 \\
&\text{BC}: \sum_{ij} \kappa_{ij}\left(\left.\frac{\partial \sigma_{ij}(x,t)}{\partial x}\right|_{x=x_r} + G_{ij}\right)\cdot n_r = 0, \quad t > 0 \\
&\text{BC}: \kappa_{ij}\left(\left.\frac{\partial \sigma_{ij}(x,t)}{\partial x}\right|_{x=x_b} + G_{ij}\right) = 0, \quad t > 0 \\
&\text{IC}: \sigma_{ij}(x,0) = \sigma_{ij,T}
\end{aligned} \tag{1}$$

where ij denotes a branch connected to nodes i and j, n_r represents the unit inward normal direction of the interior junction node r on branch ij, the value of which is $+1$ for right direction and -1 for left direction of the branch with assumption of $x_i < x_j$, $G = Eq*/\Omega$ is the EM driving force, and $\kappa = D_a B\Omega/(k_B T)$ is the diffusivity of stress. E is the electric field and $q*$ is the effective charge. $D_a = D_0 \exp(-E_a/(k_B T))$, which is the effective atomic diffusion coefficient. D_0 is the preexponential factor, B

Authorized licensed use limited to: Univ of Calif Riverside. Downloaded on June 24,2026 at 00:43:07 UTC from IEEE Xplore. Restrictions apply.

is the effective bulk elasticity modulus, Ω is the atomic lattice volume, k_B is Boltzmann's constant, T is the absolute temperature, and E_a is the EM activation energy. σ_T is the initial thermal-induced residual stress.

For a single wire with material-blocking BC, Korhonen *et al.* [17] have found the closed-form solution. Recently, Chen *et al.* [4], [25] proposed an analytic solution for multisegment interconnect wires using the Laplace transformation-based method. However, this method is only limited to a few common wire patterns such as straight s-terminal wires, T-shaped four terminal wires, and cross-shaped five terminal wires. Later on, Wang *et al.* [18] proposed a more general solution for straight multisegment wires based on eigenvalues and eigenfunctions method. He further proposed an SOV method to deal with more general multisegment interconnect tree wires [19]. Abbasinasab and Marek-Sadowska [14] also proposed analytic solutions of stress in the multisegment interconnect wires. However, this article mainly focuses on the steady-state solution of Korhonen's equation for multisegment wires, considering the temperature-induced migration effects (spatial temperature gradients are significant in interconnect wires). Authors indeed discussed the analytic solutions to the modified Korhonen's equation (with temperature-induced migration effects) using a method similar to the Laplace transformation-based method [25] and obtained the closed form for a single wire segment. However, as the work in [25] shows, it is very difficult to obtain the analytic solutions for more general multisegment wires using the Laplace transformation-based method.

B. Review of the Separation of Variables Solution for Korhonen's Equation

In this section, we briefly review the SOV method proposed in [19], which can be applied to any multisegment interconnect structures without any restrictions.

The SOV method is an analytical method to handle the typical initial-boundary value problem (IBVP). Before applying the SOV method to solve the coupled Korhonen's equations, we can homogenize both the governing equation and BCs through subtracting the transient stress distribution $\sigma(x,t)$ by the steady-state stress distribution $\sigma(x,\infty)$, which is formulated by

$$\hat{\sigma}(x,t) = \sigma(x,\infty) - \sigma(x,t). \tag{2}$$

The solutions $\sigma(x,\infty)$ for the steady-state stress problem can be obtained easily and efficiently in [2] and [7]. Using the transformation equation (2), Korhonen's equation (1) can be transformed to homogeneous IBVP, which is described by

$$\frac{\partial \hat{\sigma}_{ij}(x,t)}{\partial t} = \kappa_{ij}\frac{\partial^2 \hat{\sigma}_{ij}(x,t)}{\partial x^2}, \quad t>0 \tag{3}$$

$$\text{BC}: \hat{\sigma}_{ij_1}(x_i,t) = \hat{\sigma}_{ij_2}(x_i,t), \quad t>0 \tag{4}$$

$$\text{BC}: \sum_{ij}\kappa_{ij}\frac{\partial \hat{\sigma}_{ij}(x,t)}{\partial x}\bigg|_{x=x_r}\cdot n_r = 0, \quad t>0 \tag{5}$$

$$\text{BC}: \kappa_{ij}\frac{\partial \hat{\sigma}_{ij}(x,t)}{\partial x}\bigg|_{x=x_b} = 0, \quad t>0 \tag{6}$$

$$\text{IC}: \hat{\sigma}_{ij}(x,0) = \sigma_{ij}(x,\infty) - \sigma_{ij,T}. \tag{7}$$

After homogenization of Korhonen's equation, the SOV method is employed to obtain the general solution to (3), which is the linear combination of the product of temporal function $\Gamma_{ij,m}(t)$ and spatial distribution $\phi_{ij,m}(x)$, as given by

$$\hat{\sigma}_{ij}(x,t) = \sum_{m=1}^{\infty}\phi_{ij,m}(x)\cdot\Gamma_{ij,m}(t) \tag{8}$$

where m represents the mth component of an infinite series, temporal function

$$\Gamma_{ij,m}(t) = C_{ij,m}\cdot e^{-\lambda_{ij,m}t} \tag{9}$$

and spatial distribution

$$\phi_{ij,m}(x) = A_{ij,m}\sin(\omega_{ij,m}x) + B_{ij,m}\cos(\omega_{ij,m}x) \tag{10}$$

with the notation $\omega_{ij,m}$ defined by

$$\omega_{ij,m} = \frac{\lambda_{ij,m}}{\sqrt{\kappa_{ij}}} \tag{11}$$

where $\lambda_{ij,m}$ represents the mth eigenvalue on branch ij.

Then, the eigenvalues $\lambda_{ij,m}$ and coefficients $A_{ij,m}$, $B_{ij,m}$, and $C_{ij,m}$ can be determined by BCs (4)–(6) and initial conditions (7), respectively.

First, BCs (4)–(6) are used to find the eigenvalues $\lambda_{ij,m}$ and coefficients $A_{ij,m}$ and $B_{ij,m}$. By substituting the general solution (8) to continuous stress conditions (4), the values of the eigenvalues $\lambda_{ij,m}$ and coefficients $C_{ij,m}$ on all branches are the same as the following equations, respectively:

$$\begin{aligned} C_{ij_1,m} &= C_{ij_2,m} = C_m \\ \lambda_{ij_1,m} &= \lambda_{ij_2,m} = \lambda_m. \end{aligned} \tag{12}$$

Assuming $x_i < x_j$, the inward normal component of atom flux on both ends of branch ij can be calculated by

$$\begin{aligned} \begin{bmatrix} \left.\frac{\partial\phi_{ij,m}(x)}{\partial x}\right|_{x=x_i}\cdot n_i \\ \left.\frac{\partial\phi_{ij,m}(x)}{\partial x}\right|_{x=x_j}\cdot n_j \end{bmatrix} &= \begin{bmatrix} \left.\frac{\partial\phi_{ij,m}(x)}{\partial x}\right|_{x=x_i} \\ -\left.\frac{\partial\phi_{ij,m}(x)}{\partial x}\right|_{x=x_j} \end{bmatrix} \\ &= \begin{bmatrix} -\omega_{ij,m}\cot(\omega_{ij,m}l_{ij}) & \omega_{ij,m}\csc(\omega_{ij,m}l_{ij}) \\ \omega_{ij,m}\csc(\omega_{ij,m}l_{ij}) & -\omega_{ij,m}\cot(\omega_{ij,m}l_{ij}) \end{bmatrix}\cdot\begin{bmatrix}\phi_{ij,m}(x_i)\\ \phi_{ij,m}(x_j)\end{bmatrix} \end{aligned} \tag{13}$$

where l_{ij} is the length of branch ij.

To satisfy the conservation of the atom flux at junction nodes and block boundaries, substituting the equations in (12), the general solution (8), and the edge equations (13) to the BCs (5) and (6), we obtain

$$\boldsymbol{K}(\lambda_m)\cdot\boldsymbol{\phi} = \boldsymbol{0} \tag{14}$$

where $\boldsymbol{K}$ is an $n\times n$ matrix, and the vector is described by

$$\boldsymbol{\phi} = [\phi_{ij,m}(x_1), \phi_{ij,m}(x_2), \ldots, \phi_{ij,m}(x_n)]^T. \tag{15}$$

In order to solve the nonlinear transcendental equation $\det(\boldsymbol{K}(\lambda_m)) = 0$, the WW algorithm [26] is utilized to determine eigenvalues. The method is based on the following observation: the number of eigenvalues not exceeding μ is calculated by

$$N(\mu) = N_{0n}(\mu) + s\{\boldsymbol{K}^{\Delta}(\mu)\} \tag{16}$$

Authorized licensed use limited to: Univ of Calif Riverside. Downloaded on June 24,2026 at 00:43:07 UTC from IEEE Xplore. Restrictions apply.

where $\boldsymbol{K}^{\Delta}(\mu)$ is the triangular form of $\boldsymbol{K}(\mu)$ using the GE process, $s\{\cdot\}$ is a sign-count function that returns the number of negative main diagonal elements of the matrix, and the number of natural eigenvalues on decoupled branches with zero Dirichlet BCs on both ends is calculated by

$$N_{0n}(\mu) = \sum_{ij} \left\lfloor \frac{\mu \cdot l_{ij}}{\pi \sqrt{\kappa_{ij}}} \right\rfloor \tag{17}$$

where $\lfloor x \rfloor$ is the floor function that outputs the greatest integer less than or equal to x. By checking (16), we can determine the range of each eigenvalues and we can use bisection method to approach eigenvalues in an iterative way. However, this is also the major cost of the WW method. Once the eigenvalues λ_m are determined, the coefficients $A_{ij,m}$ and $B_{ij,m}$ can be calculated by BCs (4)–(6).

Second, using orthogonality of eigenfunctions and initial conditions (7), the coefficients C_m can be determined by

$$C_m = \frac{\sum_{ij} \langle \phi_{ij,m}(x) \cdot \hat{\sigma}_{ij}(x,0) \rangle}{\sum_{ij} \langle \phi_{ij,m}(x) \cdot \phi_{ij,m}(x) \rangle} \tag{18}$$

where the inner product is defined by

$$\langle f_{ij}(x) \cdot g_{ij}(x) \rangle = \int_{x_i}^{x_j} f_{ij}(x) g_{ij}(x) \mathrm{d}x. \tag{19}$$

Finally, the original transient hydrostatic stress $\sigma(x,t)$ is obtained by inverse transformation as shown in the following equation:

$$\sigma(x,t) = \sigma(x,\infty) - \hat{\sigma}(x,t). \tag{20}$$

C. Key Computing Steps in Existing SOV Method

In this SOV-based solution, the key computing step lies in (16), in which $\boldsymbol{K}(\mu)$ has to be triangularized by the GE processes many times using the WW algorithm. Specifically, the Gaussian elimination procedure has super-linear time complexity depending on the sparsity of the matrix. Here, we refer to N_G as the total number of multiplications used in GE, which determines its time complexity.

Another key step is to search eigenvalues by the bisection method. Based on the stop criterion $(\mu_{\max}/2^{N_{\text{iter}}}) \leq \epsilon$, the number of iterative steps of the bisection method is evaluated by

$$N_{\text{iter}} = \left\lceil \log_2 \left(\frac{\mu_{\max}}{\epsilon} \right) \right\rceil \tag{21}$$

where $\lceil x \rceil$ is the ceiling function that returns the greatest integer greater than or equal to x, $\mu_{\max}$ is the value of the maximum eigenvalue, and ϵ is the absolute error. Basically, N_{iter} will be bounded by a fixed number. The maximum number of the GE of the bisection method is approximated by

$$\begin{aligned} N_{\text{bisec}} &\approx N(\mu_{\max}, N_T) \cdot N_{\text{iter}} \\ &= N(\mu_{\max}, N_T) \cdot \left\lceil \log_2 \left(\frac{\mu_{\max}}{\epsilon} \right) \right\rceil \end{aligned} \tag{22}$$

where subscript "bisec" indicates the bisection method, $N(\mu_{\max}, N_T)$ is the number of eigenvalues not exceeding $\mu_{\max}$ of the interconnect tree with N_T T-junctions. Note that

Fig. 1. Straight line multisegment interconnect with $n-1$ segments.

N_{bisec} is not only related with the number of the interconnect tree T-junctions N_T but also depends on the maximum eigenvalue $\mu_{\max}$ and specific convergence accuracy ϵ. $N_{\text{bisec}} > N_T$ in general.

Therefore, the overall time complexity to estimate the eigenvalues depends on the multiplications of GE N_G and iterations of the bisection algorithm N_{bisec}, expressed as

$$\begin{aligned} N_{\text{total}} &\simeq N_G \times N_{\text{bisec}} \\ &= N_G \cdot N(\mu_{\max}, N_T) \cdot \left\lceil \log_2 \left(\frac{\mu_{\max}}{\epsilon} \right) \right\rceil. \end{aligned} \tag{23}$$

As a result, the key idea is how to reduce the computing costs associated with N_G and N_{bisec}.

III. Analytical Solutions of Eigenvalues for Special Cases

As mentioned above, the proposed SOV method provides the analytical solution of the physics-based EM model. However, eigenvalues have to be determined by the WW algorithm, which is a time-consuming numerical procedure. In this section, based on the SOV framework, we first present analytical methods to calculate the eigenvalues for two special cases, called straight line multisegment and star-structured multiterminal interconnects, which are commonly seen in the VLSI layout. In Section IV, we will present two strategies to accelerate the WW algorithm for the general case.

A. Straight Line Multisegment Interconnects

As shown in Fig. 1, 1-D straight line multisegment interconnect wire is the typical wire structure and topology in VLSI power grid networks. We notice this is the same wire structure handled by the proposed integral transform-based technique in [18]. However, in this article, we note that the general SOV method can also handle this case with analytic eigenvalues, and numerical eigenvalues computation is no longer needed.

Specifically, based on the angle transformation formula $\tan(ax+bx) = (\tan(ax)+\tan(bx))/(1-\tan(ax)\tan(bx))$, the zero points for the following equations are the same:

$$\tan(ax) + \tan(bx) = 0 \tag{24}$$

$$\tan((a+b)x) = 0. \tag{25}$$

With the BCs (4)–(6) and equivalent equations (24), (25), we have

$$\tan\left(\mu \frac{L_{\text{total}}}{\sqrt{\kappa}} \right) = 0 \tag{26}$$

where L_{total} is the total length of the wire.

The eigenvalues, which are the roots of (26), are then given by

$$\mu_i = \frac{i\sqrt{\kappa}\pi}{L_{\text{total}}}, \quad i = 1, 2, \ldots \tag{27}$$

Authorized licensed use limited to: Univ of Calif Riverside. Downloaded on June 24,2026 at 00:43:07 UTC from IEEE Xplore. Restrictions apply.

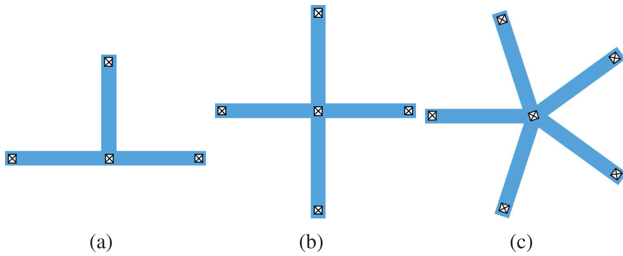

Fig. 2. Multiterminal interconnect structures: (a) four-terminal, (b) five-terminal, and (c) six-terminal.

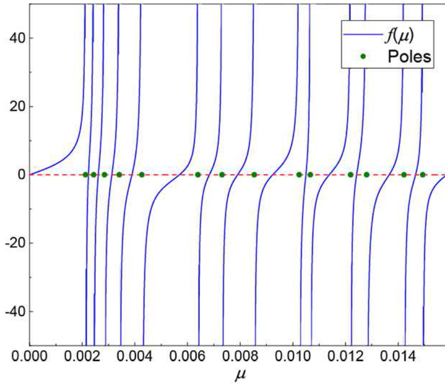

Fig. 3. Relationship between zero and pole points of the transcendental equation (28).

B. Star-Structured Multiterminal Interconnects

The second wire structure that we can solve with known eigenvalues is the star-structured multiterminal wires, as shown in Fig. 2. We notice that Chen *et al.* [4], [25] recently developed analytical solutions for stress evolution for similar star-based multiterminal interconnect structures by using the Laplace transformation technique. However, in this article, we show that the general SOV method can still solve the same wire structures with analytic eigenvalues and the start structured is also the special case of the SOV method with known eigenvalues.

Specifically, the transcendental equation to estimate the eigenvalues is given by

$$\sum_{k=0}^{N} \tan\left(\mu \frac{L_k}{\sqrt{\kappa}}\right) = 0 \tag{28}$$

where L_k is the length of the kth branches and N denotes the number of the branches in the multiterminal interconnects.

Fig. 3 shows the curve of the transcendental function, which is written by

$$f(\mu) = \sum_{k=0}^{N} \tan\left(\mu \frac{L_k}{\sqrt{\kappa}}\right). \tag{29}$$

There exists only one eigenvalue between two adjacent poles, which are shown by green dots in Fig. 3. The sequence of poles of (28) can be easily calculated by

$$\mu_p = \left(m - \frac{1}{2}\right)\frac{\sqrt{\kappa}\pi}{L_k}, \quad m = 1, 2, \ldots \tag{30}$$

Then, the elements of sequence $\{\mu_p(1), \mu_p(2), \ldots\}$ are sorted in ascending order and do not contain the same value.

Based on Cauchy's integral theorem and the use of complex integration, Luck and Stevens [27] develop a simple root-finding algorithm to formulate an explicit expression for the roots of the transcendental equations. By using the singularities of the reciprocal of the transcendental function, the method can be able to determine the zero points of the equations. With the application of the convenient method on (28), we give an analytical expression of eigenvalues, expressed as

$$\mu_i = h_i + R_i \frac{\int_0^{2\pi} w(\theta) e^{j2\theta} \mathrm{d}\theta}{\int_0^{2\pi} w(\theta) e^{j\theta} \mathrm{d}\theta}, \quad i = 1, 2, \ldots \tag{31}$$

where j denotes the imaginary number and the function $w(\theta)$ is defined as

$$\begin{aligned} w(\theta) &= \frac{1}{f(\mu)}|_{\mu = h_i + R_i e^{j\theta}} \\ &= \frac{1}{\sum_{k=0}^{N} \tan\left((h_i + R_i e^{j\theta})\frac{L_k}{\sqrt{\kappa}}\right)}. \end{aligned} \tag{32}$$

With the relationship between zero and pole points of (28), the radius and center of the closed path are, respectively, determined by

$$\begin{aligned} R_i &= \frac{\mu_p(i+1) - \mu_p(i)}{2} \\ h_i &= \mu_p(i) + R_i. \end{aligned} \tag{33}$$

By using Fourier transformation, the nth Fourier series coefficient for any $x(t)$ is calculated by

$$A_n = \frac{1}{2\pi}\int_0^{2\pi} x(t) e^{jnt} \mathrm{d}t. \tag{34}$$

It can be observed that the term $(\int_0^{2\pi} w(\theta)e^{j2\theta}\mathrm{d}\theta)/(\int_0^{2\pi} w(\theta)e^{j\theta}\mathrm{d}\theta)$ in (31) is equal to the ratio of the second Fourier series coefficient over the first one for the function $w(\theta)$. Fourier series coefficients can be efficiently calculated by using fast Fourier transform (FFT). Therefore, it is very convenient to determine the eigenvalues explicitly.

IV. Proposed Accelerated SOV for Dynamic EM Stress Analysis

For general multisegment interconnect wires with arbitrary topology, one has to find the eigenvalues using the numerical method. In this section, we try to improve the efficiency of computing eigenvalues, which is the key step in the SOV framework for solving EM-induced stress.

In the new SOV method, called the ASOV method, the basic idea is to reduce N_G and N_{bisec} by means of linear-time GE and more efficient determinant-based secant for finding eigenvalues. We will illustrate the two major ideas in this section.

A. Proposed Linear-Time Gaussian Elimination for Banded Matrices

Based on the general solutions and BCs, we first observe that $\boldsymbol{K}$ is a real symmetric matrix. In the process of GE,

Authorized licensed use limited to: Univ of Calif Riverside. Downloaded on June 24,2026 at 00:43:07 UTC from IEEE Xplore. Restrictions apply.

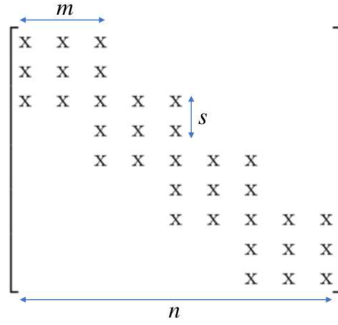

Fig. 4. Banded and step-type symmetric matrix.

Algorithm 1 Fast Linear-Time GE

Data: Transcendental matrix $\boldsymbol{K}$, bandwidth m, and step size s.
Result: Upper triangular matrix $\boldsymbol{K}^{\Delta}$.

1 **for** $i \leftarrow 1$ **to** $n-(m-s)$ **do**
   /* Move the $m \times m$ block by s rows and s columns due to the step type structure */
2   **if** $mod(i,s) == 0$ **then**
3     $p = i$;
4   **end**
   /* Do Gaussian elimination of $m \times m$ block */
5   $r = -1/K_{ii}$;
6   **for** $j \leftarrow i+1$ **to** $p+m-1$ **do**
7     $f = K_{ij} r$;
     /* Eliminate upper triangular matrix due to the symmetric structure */
8   **for** $k \leftarrow j$ **to** $p+m-1$ **do**
9       $K_{jk} = K_{jk} + f K_{ik}$;
10   **end**
11   **end**
12 **end**

each reduced matrix is also symmetric so that only the upper triangular part needs to be recorded and calculated. Therefore, the time of triangulation of a symmetric matrix is cut in half in contrast to a common matrix.

Second, for treelike structures, we further observed that $\boldsymbol{K}$ commonly is a banded and stairlike matrix with bandwidth m and step size s, as shown in Fig. 4. K_{ij} denotes the ith row and jth column of $\boldsymbol{K}$. For such matrix, the area of Gaussian elimination can be constrained in an $m \times m$ nonzero block with a shift of s rows and s columns [28]. As a result, huge products involving zero elements can be avoided, and such a banded serrated-edge matrix can be solved more efficiently by Algorithm 1.

In order to characterize the efficiency of Algorithm 1, the detailed study [28] gives an expression

$$N_{fG}(n) = a(n-b) + c \tag{35}$$

where N_{fG} denotes the total number of multiplications used in the fast GE algorithm, $a = 1 + (1/s)\sum_{i=m-s}^{m-1}[i + (i(i+1)/2)]$, $b = m - s$, and $c = \sum_{i=1}^{m-s-1}(1 + i + (i(i+1)/2))$ are constants, which depend on bandwidth m and step size s.

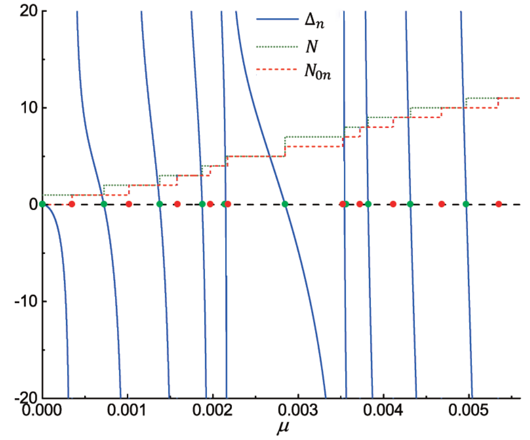

Fig. 5. Relationship between the determinant $\Delta_n(\mu)$, number of eigenvalues $N(\mu)$, and number of natural eigenvalues $N_{0n}(\mu)$.

For N_T T-junctions interconnect structure shown in Fig. 8, we have $m = 3$ and $s = 2$. By using formula (35), the computational complexity of fast GE is linear, expressed as

$$N_{fG}(n) = 4.5(n-1) \tag{36}$$

so that the triangulation of the matrix can be solved very efficiently. We remark that the general multisegment wire tree structures will always lead to such banded, serrated-edge matrix structure, suitable for the proposed GE method.

B. Proposed Fast Determinant Secant Method

The second improvement comes from a fast eigenvalues estimation strategy. Instead of using the brutal-force bisection method in WW algorithm, more efficient secant method is applied. The secant method is essentially the finite difference Newton–Raphson method. As a result, we will have a superlinear convergence. The new method consists of two main stages, including eigenvalues separation stage and subinterval iteration stage.

In the secant method, we first need to find the interval or the lower and upper bounds of the interval having only one eigenvalue and confirm the continuity of the transcendental matrix determinant in the interval, which is the eigenvalues separation stage. Let $N(\mu)$ be the number of eigenvalues not larger than μ], where μ is the eigenvalue space variable. Fig. 5 shows the relationship between $\Delta_n(\mu)$, which is the determinant value of matrix $\boldsymbol{K}$ (to be explained later), $N(\mu)$, and $N_{0n}(\mu)$. The value of $N(\mu)$ changes at the zero points, and the step jump of $N_{0n}(\mu)$ is produced at the pole points [29]. Assuming that μ_i is separated from its adjacent eigenvalues μ_{i-1} and μ_{i+1} with the lower bound μ_l and the upper bound μ_u, we have

$$\mu_{i-1} < \mu_l < \mu_i < \mu_u < \mu_{i+1} \tag{37}$$

where μ_i denotes the ith eigenvalue. To satisfy the requirement (37), the numbers of eigenvalues at lower and upper bounds have the relationship, represented by

$$N(\mu_u) = N(\mu_l) + 1. \tag{38}$$

Authorized licensed use limited to: Univ of Calif Riverside. Downloaded on June 24,2026 at 00:43:07 UTC from IEEE Xplore. Restrictions apply.

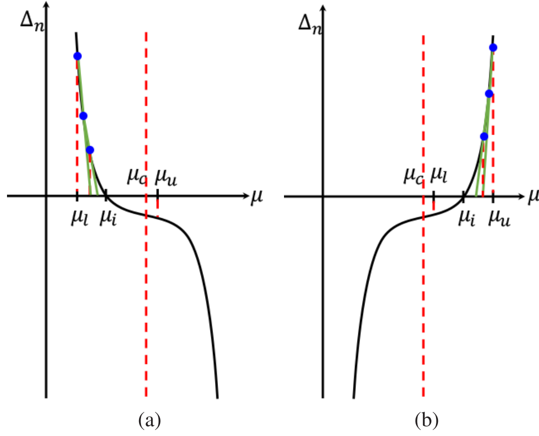

Fig. 6. Relationship between determinant Δ_n and μ in two cases: (a) $\mu_i < \mu_c$ and (b) $\mu_i > \mu_c$.

Second, we have to ensure that the determinant has no poles between μ_l and μ_u. The poles lead to discontinuity of determinant and are generated as the number of natural eigenvalues $N_{0n}(\mu)$ changes. Therefore, no pole check is given by

$$N_{0n}(\mu_l) = N_{0n}(\mu_u). \tag{39}$$

In this stage, the simple bisection procedure is employed to subdivide the interval until the obtained lower and upper bounds meet the two requirements, i.e., the eigenvalue check (38) and no pole check (39).

After this, we use the secant method to find an eigenvalue. For the secant method, similar to the Newton–Raphson method, we need to find the approximate derivative to estimate the next step. For each subinterval, the curve of the determinant is "S" like, as shown in Fig. 6. There are two possible situations: the eigenvalue locates in the left side or right side of the center μ_c, which is the center of two adjacent poles. If the eigenvalue is below μ_c, then $x_0 = \mu_l$ and $x_1 = x_0 + \delta$, where δ is a small value. Otherwise, $x_0 = \mu_u$ is chosen and $x_1 = x_0 - \delta$. Then we can find $x_{i+1} = x_i - (x_i - x_{i-1})/(\Delta_n(x_i) - \Delta_n(x_{i-1}))\Delta_n(x_i), (i = 1, 2, \ldots)$ to obtain the approximated sequences $\{x_0, x_1, x_2, \ldots\}$. The iteration of the secant method stops when $|\Delta_n|$ is equal or approximate to zero. In rare cases, the secant iteration procedure fails to obtain an eigenvalue, so we then have to continue to use the bisection method.

In addition to the computation costs savings from the secant method mentioned before, we can further reduce the computing costs associated with determining the roots of $|\boldsymbol{K}(\mu)|$. Specifically, the key computing step in the secant method is to compute the number of eigenvalues $N(\mu)$ for a given μ and compute the determinant value of the $\Delta_n(\mu) = |\boldsymbol{K}(\mu)|$, which can be obtained by multiplying the diagonal elements when it was triangularized

$$\Delta_n(\mu) = |\boldsymbol{K}(\mu)| = \prod_{i=1}^{n} a_i \tag{40}$$

where $a_i (i = 1, 2, \ldots, n)$ are the leading diagonal elements of $\boldsymbol{K}^{\Delta}$. Furthermore, If we find μ_i to make determinant $\Delta_n(\mu_i)$ equal to zero, these μ_i are the eigenvalues.

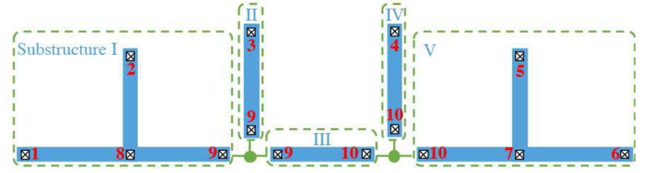

Fig. 7. Substructure procedure for the interconnect tree with 4 T-junctions.

It turns out that the two computing steps are related and can be further accelerated. One important observation is that $N(\mu)$ and $\Delta_n(\mu)$ computations are not unique (although the results are the same) and depends on how we define the building blocks of the interconnect trees. Specifically, based on (16), the total number of eigenvalues consists of the number of eigenvalues of decoupled substructures N_{0n} and that of the upper triangular matrix $\boldsymbol{K}^{\Delta}$.

We illustrate this concept in Fig. 7, which consists of five substructures (or decoupled subsystems) named I to V. At nodes 9 and 10, we divide the whole interconnect tree structure into five substructures, each of which can be solved individually and has the corresponding eigenvalues. The substructure concept is very similar to the domain decomposition method. After partitioning, we can compute the eigenvalues for each substructure and the top level structure, which only has two nodes (nodes 9 and 10 in this case). $\boldsymbol{K}$ becomes a 2×2 matrix $\boldsymbol{K}_2$ [30]

$$\boldsymbol{K}_2 \cdot \begin{bmatrix} \phi_9 \\ \phi_{10} \end{bmatrix} = \boldsymbol{0}. \tag{41}$$

By applying the WW algorithm, the number of eigenvalues not exceeding μ is given by

$$N(\mu) = N_{02}(\mu) + s\{\boldsymbol{K}_2^{\Delta}(\mu)\} \tag{42}$$

where the number of eigenvalues for substructures has five components (as we have five substructures)

$$N_{02}(\mu) = N_I(\mu) + N_{II}(\mu) + N_{III}(\mu) + N_{IV}(\mu) + N_V(\mu) \tag{43}$$

$$s\{\boldsymbol{K}_2^{\Delta}\} = \sum_{i=9}^{10} s\{a_i\} \tag{44}$$

$$\Delta_2(\mu) = |\boldsymbol{K}_2(\mu)| = \prod_{i=9}^{10} a_i. \tag{45}$$

It is was shown that the zero points for Δ_n in (40) from the original system and Δ_2 are the same [29]. As a result, we just need to compute Δ_2 as far as finding zeros (eigenvalues) are concerned.

In fact, we can partition the whole system in such a way that we only keep one node at the top, and the substructure consists of all the rest of the nodes and branches. Then, $\boldsymbol{K}_1$ becomes a 1×1 matrix or a scalar. Then, we have

$$N(\mu) = N_{01}(\mu) + s\{\boldsymbol{K}_1^{\Delta}\} = N_{01}(\mu) + s\{a_n\} \tag{46}$$

$$\Delta_1(\mu) = |\boldsymbol{K}_1(\mu)| = a_n \tag{47}$$

Authorized licensed use limited to: Univ of Calif Riverside. Downloaded on June 24,2026 at 00:43:07 UTC from IEEE Xplore. Restrictions apply.

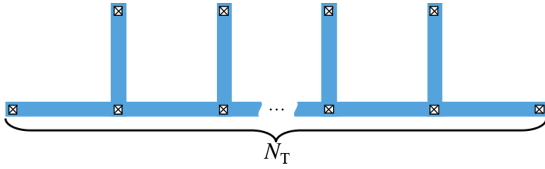

Fig. 8. N_T T-junctions interconnect structure.

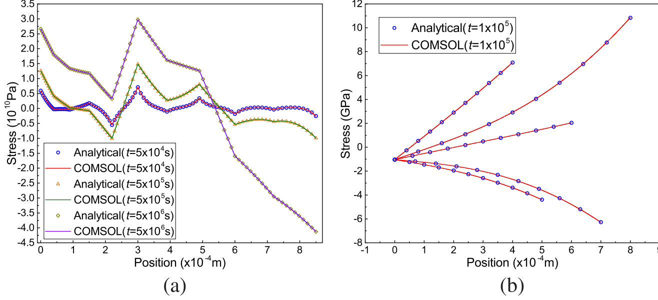

Fig. 9. Hydrostatic stress evolution of (a) ten-segment and (b) six-terminal interconnect structures.

where

$$N_{01}(\mu) = N_{0n}(\mu) + \sum_{i=1}^{n-1} s\{a_i\}. \quad (48)$$

As we can see, computing Δ_1 becomes very trivial as it is actually equivalent to the last diagonal element, a_n, during the GE process. Again, Δ_1 and Δ_n have equivalent zeros. As a result, we do not need to explicitly compute Δ_n, which leads to significant computing saving, as shown in Section V.

V. Numerical Results and Discussion

In this section, we present some numerical results and validate both the accuracy and efficiency of the ASOV method. First, we use two simple cases such as ten-segment wires and six-terminal interconnect tree to demonstrate the accuracy of analytical eigenvalues, which is compared with the WW algorithm. Then, a number of T-junction interconnect structures shown in Fig. 8 are utilized to illustrate the impact of the number and accuracy of eigenvalues on the existing SOV method. Furthermore, we compare the proposed ASOV method against the conventional SOV method. All programs are implemented in C++ and tested on a standard computer with a 2.7-GHz i5 CPU, 8-GB memory, and macOS operating system.

A. Validation of Analytical Eigenvalue Formula

For validation, ten-segment wires and six-terminal interconnect tree are simulated by the analytical eigenvalues method. Fig. 9(a) shows the hydrostatic stress distribution for the ten-segments wire with current densities as $j_1 = 4 \times 10^9$ A/m^2, $j_2 = 2 \times 10^9$ A/m^2, $j_3 = 1 \times 10^9$ A/m^2, $j_4 = 3 \times 10^9$ A/m^2, $j_5 = -5 \times 10^9$ A/m^2, $j_6 = 4 \times 10^9$ A/m^2, $j_7 = 2 \times 10^9$ A/m^2, $j_8 = 6 \times 10^9$ A/m^2, $j_9 = 3 \times 10^9$ A/m^2, and $j_{10} = 2 \times 10^9$ A/m^2. Fig. 9(b) shows the transient stress evolution for the six-terminal interconnect with current densities as $j_1 = -4 \times 10^9$ A/m^2, $j_2 = 2 \times 10^9$ A/m^2, $j_3 = -1 \times 10^9$ A/m^2, $j_4 = 3 \times 10^9$ A/m^2, and $j_5 = -5 \times 10^9$ A/m^2 at time $t = 1 \times 10^5$ s. In both cases, the results from the proposed method and commercial software COMSOL Multiphysics have a good agreement. Therefore, that is to say, the accuracy of eigenvalues is good enough to estimate the hydrostatic stress.

TABLE I
Accuracy of Eigenvalues

nth eigenvalue	Analytical Method ($L = 16$)	WW Algorithm ($\epsilon = 1 \times 10^{-11}$)	Rel. Err.
1	0.00223689427	0.00223689806	0.00017%
2	0.00261161738	0.00261161499	0.00009%
3	0.00312481621	0.00312479614	0.00064%
4	0.00388826929	0.00388816100	0.00279%
5	0.00569238397	0.00569171006	0.01184%

Table I describes the eigenvalues from analytical expression (31) and the WW algorithm. In (31), we use the FFT algorithm with the size $L = 16$ to calculate the first and second Fourier series coefficients, and the WW algorithm is employed with stop criterion $\epsilon = 10^{-11}$. As we can see, the results from analytical expression are in good agreement with that of the WW algorithm.

B. Impacts of the Number of Eigenvalues on the Accuracy of the Solutions

In order to obtain accurate transient stress, we observe that the number of eigenvalues $N(\mu_{\max}, N_T)$ should be kept constant as suggested in [19]. Instead, we find that the number of eigenvalues required for computing accurate stress using (8) depends on the structure of the interconnects. In general, more segments means more eigenvalues are needed, which leads to more computing efforts. Therefore, it is desirable to use the least number of terms possible while maintaining high accuracy in the evaluation of the series.

To illustrate the relationship between the accuracy of stress and number of eigenvalues, a number of T-junction interconnect structures, as shown in Fig. 8, were studied. The length of each branch was set to 60 μm. Under these conditions, with different number of T-junction, the eigenvalues for each term are plotted in Fig. 10. We observe that the number of eigenvalues varies periodically with increasing terms. If we obtain one period of eigenvalues, then we can obtain the infinite eigenvalues by periodic extension. For instance, the blue curve in Fig. 10 is exactly two periods of the eigenvalues for the 50-T-junction example with the eigenperiod value as μ_T, which is presented as the orange bold line. As a result, we only need one period of eigenvalues in the calculations, which captures all the useful information of the whole structure and can guarantee accuracy. In Fig. 10, the length of one period of eigenvalues is μ_T, and the number of eigenvalues increases with the number of T-junctions in one period. Therefore, as a rule of thumb, we just use $2N_T$ as the number of eigenvalues for structures with N_T T-junctions.

To demonstrate the accuracy of one period of eigenvalues, the transient hydrostatic stress analysis for an interconnect

Authorized licensed use limited to: Univ of Calif Riverside. Downloaded on June 24,2026 at 00:43:07 UTC from IEEE Xplore. Restrictions apply.

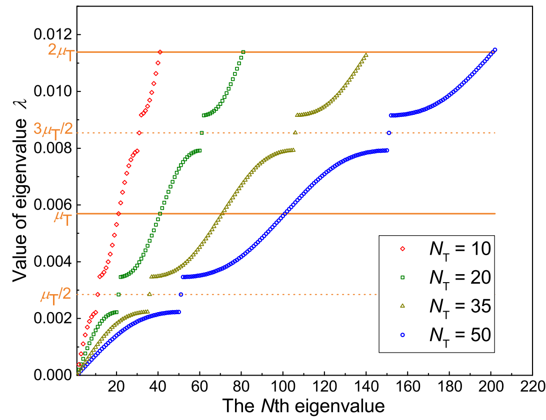

Fig. 10. Relationship between eigenvalues and number of T-junctions wires.

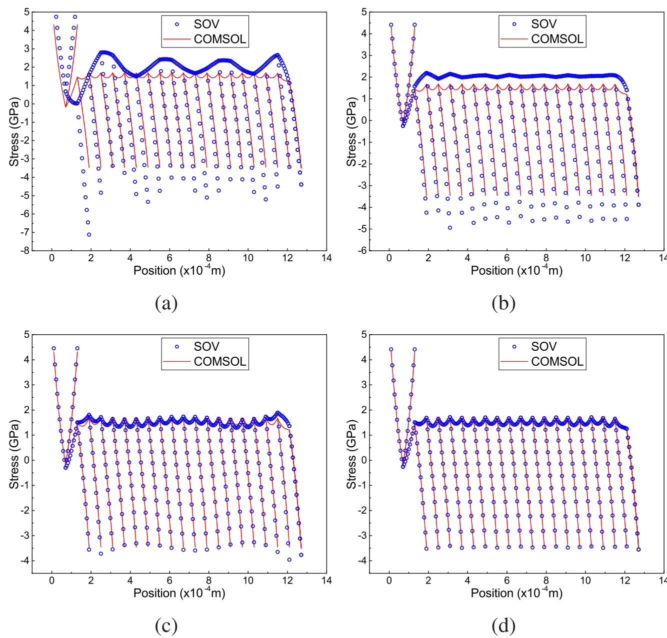

Fig. 11. Hydrostatic stress evolution of 20 T-junctions structure using (a) 8, (b) 16, (c) 24, and (d) 32 eigenvalues.

tree with 20 T-junctions is simulated by COMSOL and the SOV method. The required accuracy of the FE solution was confirmed by a fine mesh, and the SOV was simulated with different eigenvalues (8 to 32), as shown in Fig. 11. In the SOV method, the absolute error $\epsilon = 10^{-10}$ is used for stress evaluation. As we can see, the SOV methods are not accurate for the four cases (even with 32 eigenvalues).

However, if we use 40 eigenvalues, which is just twice of 20 T-junctions, the results are shown in Fig. 12. As we can see, there exists a very good agreement between the SOV and COMSOL results for stress evolution at different time points (as stress approaches the steady state).

To further illustrate the accuracy of the obtained solutions, we calculate the maximum absolute error between the SOV method and COMSOL by $\max|\sigma_{\mathrm{SOV}} - \sigma_{\mathrm{COMSOL}}|$. As shown in Table II, the maximum absolute error is reduced with the increasing number of eigenvalues. Compared with the value

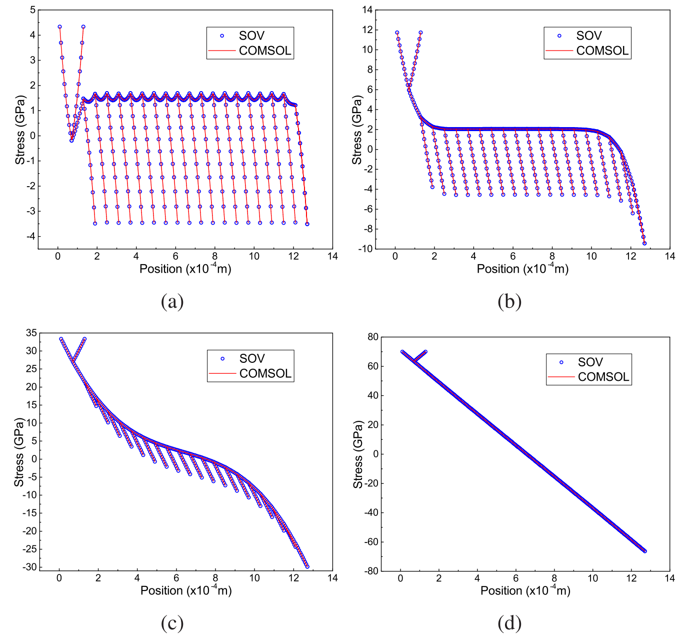

Fig. 12. Hydrostatic stress evolution of 20 T-junctions structure at (a) $t = 1 \times 10^5$ s, (b) $t = 1 \times 10^6$ s, (c) $t = 1 \times 10^7$ s, and (d) $t = 1 \times 10^8$ s.

TABLE II
IMPACT OF THE NUMBER OF EIGENVALUES ON THE ACCURACY OF THE STRESS FOR 20 T-JUNCTIONS WITH $\epsilon = 1 \times 10^{-5}$

Number of eigenvalues	Time(s)	$\max\|\sigma_{\mathrm{SOV}} - \sigma_{\mathrm{COMSOL}}\|$ (GPa)	$\frac{\max\|\sigma_{\mathrm{SOV}} - \sigma_{\mathrm{COMSOL}}\|}{\max\|\sigma_{\mathrm{COMSOL}}\|}$
8	1×10^5	3.6403	84.30%
16	1×10^5	1.4801	34.28%
24	1×10^5	0.4999	11.58%
32	1×10^5	0.1111	2.57%
40	1×10^5	0.0203	0.47%
40	1×10^6	0.0014	0.01%
40	1×10^7	0.0046	0.01%
40	1×10^8	0.0637	0.09%

of hydrostatic stress, the order of magnitude of the maximum absolute error for 40 eigenvalues is small enough to ensure the accuracy of the solution for each time point.

In addition, another main factor to determine the accuracy of hydrostatic stress is the accuracy of eigenvalues. It can be seen in Fig. 10 that the number of eigenvalues increases with the increasing number of N_T in the fixed region from 0 to μ_T, which means that the distance of the adjacent eigenvalues is reduced. Then, for the linear convergent bisection, it takes more steps to separate these eigenvalues accurately with smaller absolute error ϵ. As given in Tables II and III, we calculate the EM stress of 1000 and 20 T-junctions structure with the same $\epsilon = 10^{-10}$, $2N_T$ eigenvalues, and $t = 1 \times 10^5$ s. However, the maximum absolute error of 1000 T-junctions structure is an order of magnitude larger than that in 20 T-junctions structure. However, if we decrease the stop criterion ϵ, we get better accuracy, as described in Table III.

Above all, the accuracy of the SOV method depends on two factors, including the number and accuracy of eigenvalues, which also have a huge impact on computational time of

Authorized licensed use limited to: Univ of Calif Riverside. Downloaded on June 24,2026 at 00:43:07 UTC from IEEE Xplore. Restrictions apply.

TABLE III
IMPACT OF THE ACCURACY OF EIGENVALUES ON THE ACCURACY OF THE STRESS FOR 1000 T-JUNCTIONS AT $t = 1 \times 10^5$ s

Absolute error of eigenvalues ϵ	$\max\lvert\sigma_{\text{SOV}} - \sigma_{\text{COMSOL}}\rvert$ (GPa)	$\frac{\max\lvert\sigma_{\text{SOV}} - \sigma_{\text{COMSOL}}\rvert}{\max\lvert\sigma_{\text{COMSOL}}\rvert}$
1×10^{-10}	0.2081	4.82%
1×10^{-11}	0.0294	0.68%
1×10^{-12}	0.0275	0.64%
1×10^{-13}	0.0279	0.65%

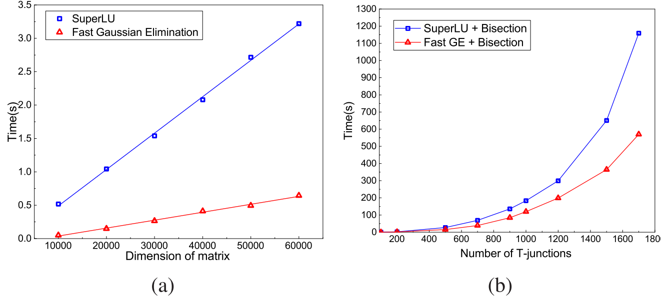

Fig. 13. (a) Comparison between SuperLU and fast GE. (b) Impact of SuperLU and Fast GE on the SOV with bisection method.

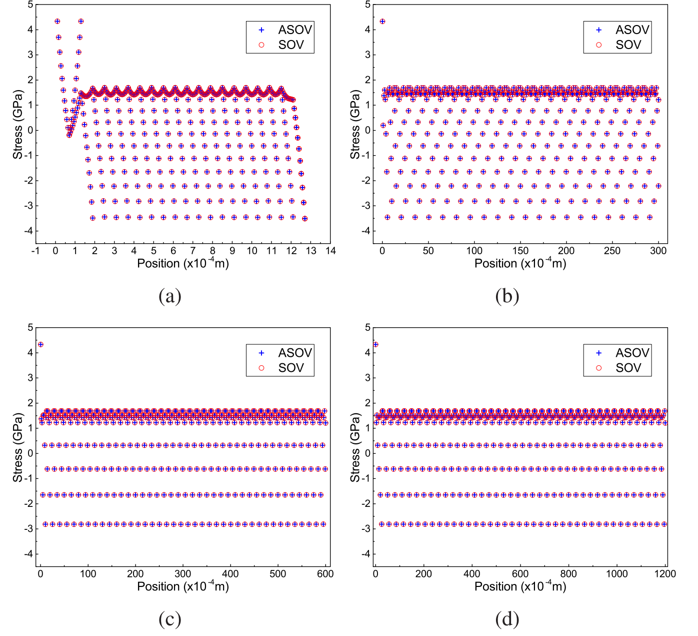

Fig. 14. Comparison of stress for (a) 20, (b) 500, (c) 1000, and (d) 2000 T-junctions computed by ASOV and SOV methods.

the WW algorithm to determine the eigenvalues. For the N_T T-junctions interconnect tree structure, the overall complexity is calculated by

$$N_{\text{total}} \simeq 2N_G \cdot N_T \cdot \left\lceil \log_2\left(\frac{\mu_{\max}}{\epsilon}\right)\right\rceil. \quad (49)$$

With the increasing number of T-junctions N_T, the required absolute error ϵ decreases. As a result, based on formula (49), the computational time to determine the eigenvalues dramatically increases.

C. Computational Efficiency Study

In order to validate the efficiency of fast GE, a sequential version of the SuperLU solver [31], [32] is used as the comparison for triangulation of $\boldsymbol{K}$ matrix. It should be noted that LU factorization routines must be configured with a diagonal pivot so that the obtained upper triangular matrix $\boldsymbol{U}$ is equal to $\boldsymbol{K}^{\Delta}$. To better collect the measurement data, we perform GE 100 times because the time consumption for a single calculation is too small to be measured.

Fig. 13(a) shows the time costs of SuperLU solver and fast GE with varying dimensions of matrix $\boldsymbol{K}$. As we can see, the computational time of both methods increases almost linearly with the size of the matrix, which means they are both scalable for the large interconnect trees. However, the proposed fast GE still has better computational efficiency compared to the general SuperLU sparse solver. We further study the impact of these GEs on the whole SOV method, and the results are shown in Fig. 13(b). As we can see that the fast GE-based SOV is about twice faster than SuperLU-based SOV.

With the improved eigenvalue searching algorithm, we can obtain better speedup as shown in the following. We demonstrate this by comparing the performance of our proposed ASOV method and the existing SOV method with the increasing number of T-junctions, N_T. The time point of the hydrostatic stress evolution is set to $t = 1\times10^5$ s. For each test case, $2N_T$ eigenvalues are used to estimate the transient stress. The results are given in Table IV. We note that the stop criteria of ASOV and SOV are different, including the absolute error ϵ for the bisection method and determinant $|\Delta_1|$ for the secant method. To obtain the hydrostatic stress with the same accuracy for fair comparison, the stop criteria of ASOV and SOV methods may be different where their accuracies will be kept equal as much as possible. Fig. 14 shows the accuracy comparison of ASOV and SOV methods for a interconnect tree for 20, 500, 1000, and 2000 T-junctions. We can observe a good agreement between the two methods. Afterward, we can compare the efficiency of the two methods. As given in Table IV, the proposed ASOV method can achieve 3–5X speedup over the existing SOV method, which is quite significant.

TABLE IV
RUNTIME COMPARISON OF THE ASOV AND SOV METHODS

N_T	SOV (sec)	ϵ	ASOV (sec)	$\lvert\Delta_1\rvert$	Speed up
20	0.0233	10^{-10}	0.0094	10^{-2}	2.5
100	0.4142	10^{-10}	0.1361	10^{-2}	3.0
500	24.079	10^{-11}	6.9650	8×10^{-3}	3.5
1000	182.78	10^{-12}	57.885	10^{-3}	3.2
2000	2464.0	5×10^{-13}	530.85	10^{-4}	4.6
5000	23136	10^{-13}	7068.2	2.5×10^{-5}	3.3

VI. CONCLUSION

In this article, we have proposed a new analytic solution to compute the stress evolution in the confined multisegment interconnect wires. The new method, called the ASOV method, aims to find the analytic solutions of the PDEs of stress in confined interconnect metals based on the SOV method. However, it offers several improvements over the

Authorized licensed use limited to: Univ of Calif Riverside. Downloaded on June 24,2026 at 00:43:07 UTC from IEEE Xplore. Restrictions apply.

existing plain SOV-based method. We first provided the analytic solutions to the eigenvalues for straight line and star-structured multisegment interconnect wires instead of computing them numerically as in the existing SOV method. We then proposed a linear GE algorithm by exploiting the banded structure with a serrated-edge form of the transcendental matrix, which can lead to better performance than the general sparse GE process. Finally, we proposed to use the enhanced determinant-based secant iterative method to find the eigenvalues of the transcendental matrix. Numerical results have shown that the resulting algorithm can achieve 3–5X speedup over the existing plain SOV-based solution on a number of multisegment interconnect benchmarks.

REFERENCES

[1] S. X.-D. Tan, M. Tahoori, T. Kim, S. Wang, Z. Sun, and S. Kiamehr, *Long-Term Reliability of Nanometer VLSI Systems-Modeling, Analysis and Optimization*. Cham, Switzerland: Springer, 2019.

[2] X. Huang, T. Yu, V. Sukharev, and S. X.-D. Tan, "Physics-based electromigration assessment for power grid networks," in *Proc. Design Automat. Conf. (DAC)*, Jun. 2014, pp. 1–6.

[3] V. Sukharev, X. Huang, H.-B. Chen, and S. X.-D. Tan, "IR-drop based electromigration assessment: Parametric failure chip-scale analysis," in *Proc. Int. Conf. Comput. Aided Design (ICCAD)*, Nov. 2014, pp. 428–433.

[4] H.-B. Chen, S. X.-D. Tan, X. Huang, T. Kim, and V. Sukharev, "Analytical modeling and characterization of electromigration effects for multibranch interconnect trees," *IEEE Trans. Comput.-Aided Design Integr. Circuits Syst.*, vol. 35, no. 11, pp. 1811–1824, Nov. 2016.

[5] X. Huang, A. Kteyan, X. Tan, and V. Sukharev, "Physics-based electromigration models and full-chip assessment for power grid networks," *IEEE Trans. Comput.-Aided Des. Integr. Circuits Syst.*, vol. 35, no. 11, pp. 1848–1861, Feb. 2016.

[6] V. Mishra and S. S. Sapatnekar, "Predicting electromigration mortality under temperature and product lifetime specifications," in *Proc. 53rd ACM/EDAC/IEEE Design Autom. Conf. (DAC)*, Jun. 2016, pp. 1–6.

[7] Z. Sun, E. Demircan, M. D. Shroff, T. Kim, X. Huang, and S. X.-D. Tan, "Voltage-based electromigration immortality check for general multi-branch interconnects," in *Proc. Int. Conf. Comput. Aided Design (ICCAD)*, Nov. 2016, pp. 1–7.

[8] X. Huang, V. Sukharev, T. Kim, and S. X.-D. Tan, "Electromigration recovery modeling and analysis under time-dependent current and temperature stressing," in *Proc. Asia South Pacific Design Autom. Conf. (ASPDAC)*, Jan. 2016, pp. 244–249.

[9] X. Huang, V. Sukharev, T. Kim, and S. X.-D. Tan, "Dynamic electromigration modeling for transient stress evolution and recovery under time-dependent current and temperature stressing," *Integration*, vol. 58, pp. 518–527, Jun. 2016.

[10] S. Chatterjee, V. Sukharev, and F. N. Najm, "Power grid electromigration checking using physics-based models," *IEEE Trans. Comput.-Aided Design Integr.*, vol. 37, pp. 1317–1330, Jul. 2018.

[11] S. X.-D. Tan, H. Amrouch, T. Kim, Z. Sun, C. Cook, and J. Henkel, "Recent advances in EM and BTI induced reliability modeling, analysis and optimization (invited)," *Integration*, vol. 60, pp. 132–152, Jan. 2018.

[12] Z. Sun, E. Demircan, M. D. Shroff, C. Cook, and S. X.-D. Tan, "Fast electromigration immortality analysis for multi-segment copper interconnect wires," *IEEE Trans. Comput.-Aided Des. Integr. Circuits Syst.*, vol. 37, pp. 3137–3150, Dec. 2018.

[13] H. Zhao and S. X.-D. Tan, " Postvoiding FEM analysis for electromigration failure characterization," *IEEE Trans. Very Large Scale Integr. (VLSI) Syst.*, vol. 26, no. 11, pp. 2483–2493, Nov. 2018.

[14] A. Abbasinasab and M. Marek-Sadowska, "RAIN: A tool for reliability assessment of interconnect networks—Physics to software," in *Proc. 55th ACM/ESDA/IEEE Design Autom. Conf. (DAC)*, Jun. 2018, pp. 1–6.

[15] C. Cook, Z. Sun, E. Demircan, M. D. Shroff, and S. X.-D. Tan, "Fast electromigration stress evolution analysis for interconnect trees using Krylov subspace method," *IEEE Trans. Very Large Scale Integr. (VLSI) Syst.*, vol. 26, no. 5, pp. 969–980, May 2018.

[16] V. Sukharev and F. N. Najm, "Electromigration check: Where the design and reliability methodologies meet," *IEEE Trans. Device Mater. Rel.*, vol. 18, no. 4, pp. 498–507, Dec. 2018.

[17] M. A. Korhonen, P. Bo-Rgesen, K. N. Tu, and C.-Y. Li, "Stress evolution due to electromigration in confined metal lines," *J. Appl. Phys.*, vol. 73, no. 8, pp. 3790–3799, 1993.

[18] X. Wang, H. Wang, J. He, S. X.-D. Tan, Y. Cai, and S. Yang, "Physics-based electromigration modeling and assessment for multi-segment interconnects in power grid networks," in *Proc. Design, Automat. Test Eur. (DATE)*, Mar. 2017, pp. 1727–1732.

[19] X. Wang, Y. Yan, J. He, S. X.-D. Tan, C. Cook, and S. Yang, "Fast physics-based electromigration analysis for multi-branch interconnect trees," in *Proc. IEEE/ACM Int. Conf. Comput.-Aided Design (ICCAD)*, Nov. 2017, pp. 169–176.

[20] J. R. Black, "Physics of electromigration," in *Proc. 12th Int. Rel. Phys. Symp.*, Apr. 1974, pp. 142–149.

[21] I. A. Blech, "Electromigration in thin aluminum films on titanium nitride," *J. Appl. Phys.*, vol. 47, no. 4, pp. 1203–1208, Apr. 1976.

[22] C. M. Tan, *Electromigration in ULSI Interconnections* (International Series on Advances in Solid State Electronics and Technology). Singapore: World Scientific, 2010.

[23] J. Lienig and M. Thiele, *Fundamentals of Electromigration-Aware Integrated Circuit Design*. New York, NY, USA: Springer, 2018.

[24] V. Sukharev, A. Kteyan, and X. Huang, "Postvoiding stress evolution in confined metal lines," *IEEE Trans. Device Mater. Rel.*, vol. 16, no. 1, pp. 50–60, Mar. 2016.

[25] C. Chen, S. X.-D. Tan, J. Peng, T. Kim, and J. Chen, "Analytical modeling of electromigration failure for VLSI interconnect tree considering temperature and segment length effects," *IEEE Trans. Device Mater. Rel.*, vol. 17, no. 4, pp. 653–666, Dec. 2017.

[26] W. H. Wittrick and F. W. Williams, "A general algorithm for computing natural frequencies of elastic structures," *Quart. J. Mech. Appl. Math.*, vol. 24, pp. 263–284, Aug. 1971.

[27] R. Luck and J. W. Stevens, "Explicit solutions for transcendental equations," *SIAM Rev.*, vol. 44, no. 2, pp. 227–233, 2002.

[28] F. W. Williams and D. Kennedy, "Fast Gauss-Doolittle matrix triangulation," *Comput. Struct.*, vol. 28, no. 2, pp. 143–148, 1988.

[29] F. W. Williams and D. Kennedy, "Reliable use of determinants to solve non-linear structural eigenvalue problems efficiently," *Int. J. Numer. Methods Eng.*, vol. 26, no. 8, pp. 1825–1841, Aug. 1988.

[30] F. W. Williams and W. H. Wittrick, "Exact buckling and frequency calculations surveyed," *J. Struct. Eng.*, vol. 109, no. 1, pp. 169–187, 1983.

[31] X. Li, J. Demmel, J. R. Gilbert, L. Grigori, M. Shao, and I. Yamazaki, "SuperLU users' guide," Lawrence Berkeley Nat. Lab., Berkeley, CA, USA, Tech. Rep. LBNL-44289, Sep. 1999. Accessed: Aug. 2011. [Online]. Available: http://crd.lbl.gov/~xiaoye/SuperLU/

[32] J. W. Demmel, S. C. Eisenstat, J. R. Gilbert, X. S. Li, and J. W. H. Liu, "A supernodal approach to sparse partial pivoting," *SIAM J. Matrix Anal. Appl.*, vol. 20, no. 3, pp. 720–755, 1999.

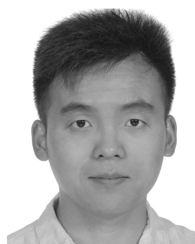

Liang Chen (S'16) was born in 1992. He received the B.E. degree in electromagnetic field and wireless technology from Northwestern Polytechnical University, Xi'an, China, in 2015. He is currently working toward the Ph.D. degree in electronic science and technology at Shanghai Jiao Tong University, Shanghai, China.

He is currently a Visiting Student at the VLSI System and Computation Laboratory, Department of Electrical and Computer Engineering, University of California at Riverside, Riverside, CA, USA. His current research interests include signal integrity of high-speed interconnects, electrothermal cosimulation of 3-D integrated packages, and electromigration reliability.

Authorized licensed use limited to: Univ of Calif Riverside. Downloaded on June 24,2026 at 00:43:07 UTC from IEEE Xplore. Restrictions apply.

Sheldon X.-D. Tan (S'96–M'99–SM'06) received the B.S. and M.S. degrees in electrical engineering from Fudan University, Shanghai, China, in 1992 and 1995, respectively, and the Ph.D. degree in electrical and computer engineering from The University of Iowa, Iowa City, IA, USA, in 1999.

He was a Visiting Professor at Kyoto University, Kyoto, Japan, as a JSPS Fellow from December 2017 to January 2018. He is currently a Professor at the Department of Electrical Engineering, University of California at Riverside, Riverside, CA, USA, where he is also a Cooperative Faculty Member at the Department of Computer Science and Engineering. His current research interests include VLSI reliability modeling, optimization, and management at circuit and system levels, hardware security, thermal modeling, optimization and dynamic thermal management for many-core processors, parallel computing, and adiabatic and Ising computing based on GPU and multicore systems. He has authored or coauthored more than 290 technical articles and has coauthored 6 books in the above-mentioned areas.

Dr. Tan was a recipient of the NSF CAREER Award in 2004, three Best Paper Awards from ICSICT'18, ASICON'17, ICCD'07, and DAC'09, and the Honorable Mention Best Paper Award from SMACD'18. He is serving as the TPC Vice Chair for ASPDAC in 2019. He is serving or served as the Editor-in-Chief for Elsevier's *Integration*, the VLSI Journal, and the Associate Editor for three journals: the IEEE TRANSACTIONS ON VERY LARGE SCALE INTEGRATION (VLSI) SYSTEMS, the *ACM Transactions on Design Automation of Electronic Systems* (TODAE), and Elsevier's *Microelectronics Reliability*.

Zeyu Sun (S'16) received the B.S. degree in electronic and computer engineering from The Hong Kong University of Science and Technology (HKUST), Hong Kong, in 2015. He is currently working toward the Ph.D. degree at the Department of Electrical and Computer Engineering, University of California at Riverside, Riverside, CA, USA.

His current research interests include electromigration modeling and assessment and reliability-aware performance optimization.

Shaoyi Peng (S'17) received the B.S. degree in microelectronics from Fudan University, Shanghai, China, in 2016. He is currently working toward the Ph.D. degree at the Department of Electrical and Computer Engineering, University of California at Riverside, Riverside, CA, USA.

His current research interests include VLSI reliability effect modeling and simulation.

Min Tang (M'09) was born in 1980. He received the B.S. degree in electronic engineering from Northwestern Polytechnical University, Xi'an, China, in 2001, the M.S. degree in electrical engineering from Xi'an Jiao Tong University, Xi'an, in 2004, and the Ph.D. degree in electronic engineering from Shanghai Jiao Tong University, Shanghai, China, in 2007.

Since 2007, he has been a Faculty Member at Shanghai Jiao Tong University, where he is currently an Associate Professor at the Department of Electronic Engineering. From 2010 to 2012, he was a Postdoctoral Research Fellow at The University of Hong Kong, Hong Kong. His current research interests include signal and power integrity of high-speed circuits and multiscale and multiphysics modeling of integrated systems.

Junfa Mao (M'92–SM'98–F'12) was born in 1965. He received the B.S. degree in radiation physics from the National University of Defense Technology, Changsha, China, in 1985, the M.S. degree in experimental nuclear physics from the Shanghai Institute of Nuclear Research, Chinese Academy of Sciences, Shanghai, China, in 1988, and the Ph.D. degree in electronic engineering from Shanghai Jiao Tong University, Shanghai, in 1992.

Since 1992, he has been a Faculty Member at Shanghai Jiao Tong University, where he is currently a Chair Professor and a Vice President. He was a Visiting Scholar at The Chinese University of Hong Kong, Hong Kong, from 1994 to 1995, and a Postdoctoral Researcher at the University of California at Berkeley, Berkeley, CA, USA, from 1995 to 1996. He has authored or coauthored more than 500 articles (including more than 130 IEEE journal articles). His current research interests include the interconnect and package problems of integrated circuits and systems, analysis, and design of microwave components and circuits.

Authorized licensed use limited to: Univ of Calif Riverside. Downloaded on June 24,2026 at 00:43:07 UTC from IEEE Xplore. Restrictions apply.